Probabilistic Evaluation for Flight Mission Feasibility of a Small Octocopter in the Presence of Wind

Ellis L. Thompson*, Abenezer Taye†, James Ashby‡, Gerald Fattah§, and Peng Wei¶
The George Washington University, Washington, D.C. 20052, USA

Timothy Bonin‖ and James Jones**
MIT Lincoln Laboratory, Lexington, MA 02421, USA

Marcos Quinones-Grueiro†† and Gautam Biswas‡‡
Vanderbilt University, Nashville, TN 37212, USA

The Advanced Air Mobility (AAM) concept envisions small unmanned aerial systems (UASs) and some larger electric vertical take-off and landing (eVTOL) vehicles operating in close proximity to one another within populated areas. As such it is important to assess the feasibility of a mission before departure. This includes both the aircraft's ability to maneuver to each waypoint safely, as well as ensuring that the aircraft can perform the mission given some initial State of Charge (SoC). Both of these performance related assessments can be affected by the presence of wind by either observing deviations from the prescribed flight plan or an increase in anticipated power consumption, draining the battery. In this paper we outline two systems developed to probabilistically evaluate the feasibility of a flight for a small UAS octocopter in the presence of wind. Designed in two parts, the first evaluates flight plan conformance identifying regions of deviation above a provided threshold. The second evaluates mission feasibility based on battery performance and yields a probability of completion given the remaining state of charge.

Nomenclature

A	=	Propeller area
C_D	=	The drag coefficient of the aircraft body
C_{H_i}	=	The drag coefficient of the ith rotor
D	=	Deviation threshold distance
d	=	Distance from a given point to the closest point on a prescribed flight plan segment
F_D^{Total}	=	The total drag force acting on the aircraft
$F_D^{airframe}$	=	The drag force acting on the air frame
F_D^{prop}	=	The drag force acting on the propellers
k	=	The discrete time variable
R	=	Propeller diameter
S	=	Aircraft cross-sectional area
$u(k)$	=	Input vector
V	=	Aircraft velocity
$v(k)$	=	Process noise vector

*Graduate Research Assistant, Department of Computer Science, School of Engineering and Applied Science, AIAA Member.

†Graduate Research Assistant, Mechanical and Aerospace Engineering Department, School of Engineering and Applied Science, AIAA Member.

‡Undergraduate Student Researcher, Mechanical and Aerospace Engineering Department, School of Engineering and Applied Science

§Undergraduate Student Researcher, Mechanical and Aerospace Engineering Department, School of Engineering and Applied Science

¶Assistant Professor, Mechanical and Aerospace Engineering Department, School of Engineering and Applied Science, AIAA Senior Member.

‖Technical Staff, Air Traffic Control Systems Group, AIAA Member

**Technical Staff, Air Traffic Control Systems Group, AIAA Senior Member

††Research Scientist, Institute for Software Integrated Systems

‡‡Professor, Computer Science Department

$\mathcal{W}$	=	The set of ordered waypoints belonging to a route
w_n	=	The nth waypoint such that $w_n \in \mathcal{W}$
$x(k)$	=	The state vector
$y(k)$	=	Output vector
$\theta(k)$	=	The unknown parameter vector
ρ	=	Air density
Ω	=	Propeller RPM

I. Introduction

In our previous work [1], we identified potential hazards to both aircraft and the airspace within the Advanced Air Mobility (AAM) concept. In this research we have focused on hazards imposed by wind on both: flight plan conformance, if the aircraft is predicted to deviate from its filed flight plan, as well as, on the battery, if there is sufficient charge to complete a flight. As an example, [2] considers the Unmanned Aerial Vehicle (UAV) operation in urban environments while taking the battery energy into account. While existing research looks at both the effect of wind on rigid body UAVs as well as wind-optimal trajectory planning for electric Vertical Take Off and Landing vehicles (eVTOLs) [3, 4], we are concerned with a middle ground, evaluating how much an aircraft may deviate from a given provided path due to the effect of wind. This paper presents two systems for examining the effect of wind on a vehicles ability to complete a flight considering both deviation from a planned route as well as the depletion of battery charge. Additionally, we evaluate these systems in both an environment with deterministic forecast winds from the Dallas Fort-Worth area, as well as, real observed winds from the Centreville, Virginia area.

The proposed system exists as part of a larger architecture, shown in Figure 1, as part of an in-time learning-based aviation safety management system (ILASMS), referenced in [1], and is designed around a pre-flight, joint-probability approach to evaluate mission feasibility. The remainder of the paper is structured as follows, Section II covers related literature. In Section III we outline the simulation environment used along with the parameters of the aircraft. Section IV outlines the approach used to generate a conformance metric and Section V covers the approach to predicting the feasibility of the mission given the impact of wind on the battery. In Section VI an overview of the experiments conducted and their findings are presented and finally, Section VII provides concluding remarks.
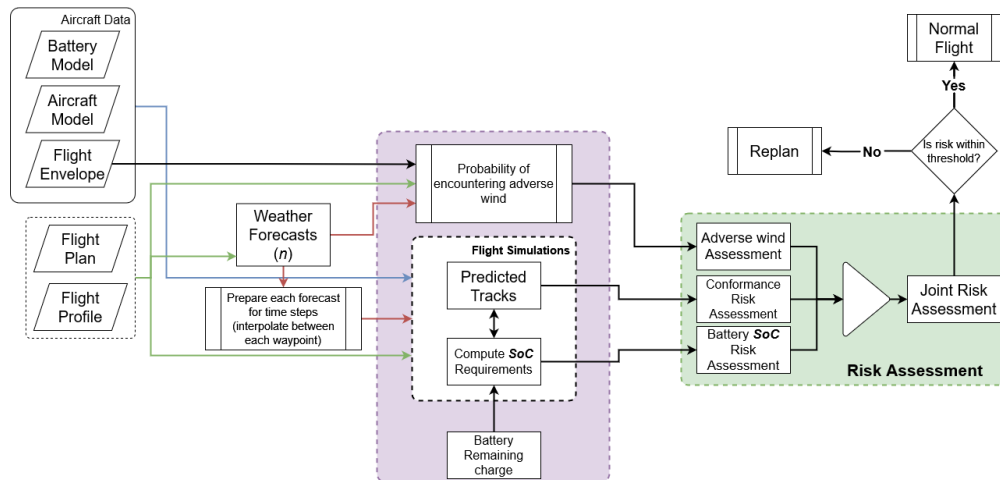
Fig. 1   A conceptual breakdown of the larger proposed architecture for evaluating mission feasibility given a flight plan and battery and aircraft parameters. The first box (purple) focuses on generating individual probabilities for wind encounters, conformance and completion given battery State of Charge (SoC), while the second box (green) performs a joint probability risk assessment based on these values and some threshold.

II. Related Literature

A. Modelling Aircraft in the Presence of Wind

Exhaustive research exists in the domain of modelling the effects of wind on aircraft. In [5], the approach used focuses on applying the drag forces on the aircraft in the presence of wind. The approach references the wind in the aircraft's body frame of reference and then uses the drag equation to calculate parasitic drag on the aircraft. The control infrastructure of the aircraft then uses this resultant force to attempt to compensate for the wind at the control level. An alternative approach [6], uses the *Dryden Wind Turbulence* model [7] for including wind into the aircraft model. Additionally, in this approach, the overall approach examines both the aircraft and wind speed from a ground reference frame rather than in the frame of the aircraft.

In the works [8–10] the real effects of wind on the aircraft were considered, that is the data on the drag coefficients and resultant drag were calculated through physical experiments. In [9], these values were used to generate a *safe flight envelope*, or the performance area the aircraft can safely operate under. Again, using data obtained through physical experiments, [8] examines trajectory prediction with off-nominal flight dynamics. This approach looks at identifying failure conditions for aircraft but does not focus directly on the effect wind alone has.

B. Probabilistic Evaluation of Flight Plan Deviation

Evaluation of flight plan deviation can be split into two broad sections: Dynamic Weather Reroutes (DWR) [11], which attempts to automatically regenerate paths around adverse weather for in-flight aircraft; and strategic trajectory prediction, a second ground-based tool designed to operate with a long-forecast look ahead. The Terminal AutoResolver [12] is a DWR approach that uses an algorithm to path around a convective weather polygon by adding a single auxiliary waypoint [13]. In [14], a recurrent neural network is used to predict a trajectory given some weather features.

Strategic trajectory prediction, often occurring preflight or with a significant look ahead, employs similar strategies. However, rather than only aiding in on-route operations, such tools can be used with general traffic management, efficient utilization or airfield resources in conjunction with weather avoidance [15–20]. Approaches in strategic trajectory prediction focus on the prediction of the trajectory either from historically gathered trajectory data or simulated predictions. Additionally, the evaluation of these trajectories can be both statistical in nature or employ neural network approaches like recurrent neural networks and long short-term memory [21].

C. Battery Energy related Flight Planning

Several previous studies have explored the impacts of battery energy on the operational decision-making of autonomous systems. Sweet et al. [22] investigated the influence of battery state of charge on the route planning of ground mobile robots, while Daigle [23] discussed the End-of-Discharge (EoD) voltage prediction procedure for a single-cell battery. Corbetta et al. [24] presented a framework to quantify uncertainty in mission success due to available battery energy, but only considered the power train model of a UAV. Quinones-Grueiro et al. [2] studied the UAV navigation problem in urban environments while taking the battery energy into account. Priyank et al. [25] used an optimal control framework for a multi-rotor eVTOL aircraft to achieve energy-efficient arrival with a required time of arrival constraint, and [26] proposed an approach to generate wind-optimal trajectories for UAM missions with minimum energy consumption. Additionally, Schumann et al. [27] introduced a prognostics-as-a-service (PaaS) framework for UAVs that monitors the health and state of charge of the battery (SoC), among other features of the UAV online, communicates the state of the aircraft to ground controllers, and can perform contingency planning. However, none of these studies take into account complex aircraft and battery dynamic models, nor do they consider actual wind forecasts. Therefore, this paper presents a comprehensive framework to examine the influence of battery energy on flight missions.

III. The Simulation Environment

The work presented relies heavily on evaluation from simulated data. In this work we utilized the simulation environment written in Python provided in [28]. Additionally, we based the octocopter model on the Tarot T18 [29] using the parameters in Table 1.

A predetermined route ($\mathcal{W}$) is supplied to the simulation consisting of waypoints $w \subset \mathbb{R}^3$ which are 3-dimensional points within the airspace. As the simulation runs, at each time-step, the state of the aircraft is recorded which includes the position, roll, pitch and yaw as well as the speeds and the currents and voltages at the motors. The recorded data is

then evaluated for flight plan conformance as well as probability of completion given the calculated battery SoC.

Table 1   Parameters of the simulated vehicle

Parameter	Value
Mass (kg)	10.66
Diameter (m)	1.25
Elliptical Area (m^2)	4.023
N Propellers	8
Propeller Distance (m)	0.635
Max Voltage (V)	22.2
Max Current (A)	38.0

IV. Predicting Flight Plan Conformance

To predict flight plan conformance, we need to evaluate if the aircraft deviates from the assigned series of waypoints in the presence of wind. To expand further, if the set of successive waypoints is defined as $\mathcal{W} = \{w_0, w_1, ..., w_n\}$, then for a given waypoint $w_m \in \mathcal{W}$, the aircraft must fly over w_{m-1} before w_m. The path between w_{m-1} and w_m can therefore be considered as the reference trajectory. Deviation then occurs when, at any given time t_n, the distance from the aircraft's actual position to the reference trajectory exceeds some threshold D. Finally, the conformance metric describes this deviation for a collection of pre-flight simulated scenarios where the aircraft operates in an environment with predicted winds. To evaluate conformance then three steps present themselves beyond the initial route generation: (1) Collect a series of wind predictions over the area of the desired route; (2) Simulate the aircraft operating in the environment with the applied relevant winds; (3) Describe the relative deviations as a *conformance* metric or rather probability of significant deviation occurring.

A. Generating the Wind Forecast Data

A micro-wind service was developed to provide wind forecast information to support the flight planning needs of flight operators and other low-altitude aviation stakeholders. The Weather Research and Forecasting (WRF) [30] model was used to generate high-resolution deterministic wind forecasts. The model simulates weather conditions by solving a set of partial differential equations and produces three-dimensional gridded volumes of wind forecasts and other weather products. The model was configured to provide forecasts for the Dallas Fort-Worth area every 15 minutes at a horizontal resolution of $100m \times 100m$. The forecast data was utilized by a server that could provide forecast wind values at discrete locations when queried over the internet. An application public interface was set up to allow external users to interact with the service by making individual request for data. Users can specify the points along a four-dimensional trajectory that they intend to fly, and the service will provide them with the weather forecast information to estimate the wind speed and direction at the requested points by interpolating the data at the requested spatial and temporal locations.

## B. Converting Wind Speed to Drag Values

In this paper we primarily focus on the effect of parasitic drag on the vehicle. This is the drag experienced on an object as it moves through a fluid, in this instance air. We are able to calculate the total drag by using Equations 1 and 2 resulting in: $F_D^{Total} = F_D^{airframe} + F_D^{prop}$, where ρ is the supplied air density, V is the relative velocity, S is the cross-sectional area of the aircraft and A the propeller area. Ω and R are the propeller RPM and diameter respectively.

$$F_D^{airframe} = \frac{1}{2}\rho V^2 S C_D \tag{1}$$

$$F_D^{prop} = \rho A (\Omega R)^2 C_{H_i} \tag{2}$$

The drag coefficents along with the drag forces at different velocities were precalculated as outlined in [8–10]. This yields a look-up table to provide an estimation of the drag acting on the aforementioned components or the

drag coefficients if required as demonstrated in Figure 2. This was modeled in python code to match the simulation environment. These precalculated values were generated using a smaller model of aircraft compared to what is used in the simulations. As such a scaling value is required to ensure the correct values are obtained for the drags. Table 2 shows the diameter and area difference between the two Tarot vehicles. The TX8 [31], was used to calculate the values and the T18 [29], was used in our simulation tests.
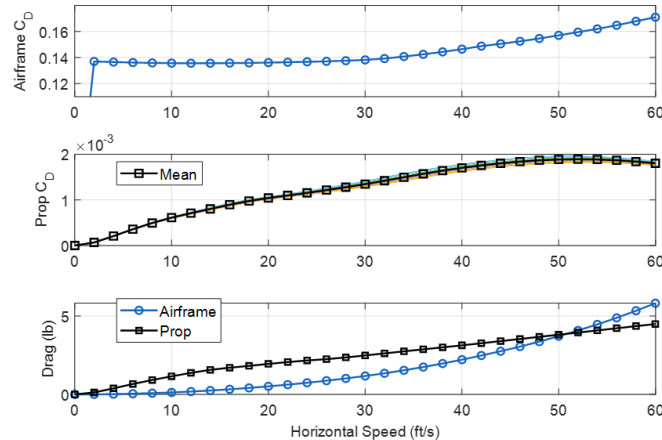
Fig. 2   The drag coefficients and resultant drag forces were precalculated. The top two graphs show the air frame and Prop drag coefficients respectively. The bottom graph shows the relative drag forces at varying speeds.

Table 2   A comparison between the Tarot X8 and T18 vehicles

	Tarot X8 [31]	Tarot T18 [29]
Motor-to-motor diameter (m)	0.969	1.250
Top-down elliptical area (m)	2.426	4.023

The resultant algorithm accepts a given wind speed as well as angle of attack and vehicle speed, obtained through the simulation. It then uses these values to obtain the total drag force (F_D^{Total}) acting on the aircraft. Additional functionality allows for the user to specify the air density and humidity. Exploration of this however remained outside the scope of this project and so we will not go into more detail on this topic in the paper.

C. Evaluating Conformance

Three methods for evaluating flight path conformance are presented in this paper: (1) Strict conformance boundaries; (2) Evaluation of conformance over the entire route; (3) Statistical evaluation of conformance over finite time intervals.

1. Strict conformance boundaries

The first approach we present is also the most intuitive. At the point of evaluation, the resultant simulation trace, with the predicted winds, is examined for recorded points that exist above a threshold. If a point lies without this predefined threshold, then it is declared that conformance is broken and a re-plan is required. In reality this is run in line with the simulation and at the point conformance is not met the simulation is terminated.

This approach is reminiscent of the Required Navigation Performance (RNP) procedures outlined in [32]. This approach however does not take into account the uncertainty that is inherent with the wind forecast. This uncertainty could cause the approach to potentially return a greater number of false negatives proving to be overly conservative.
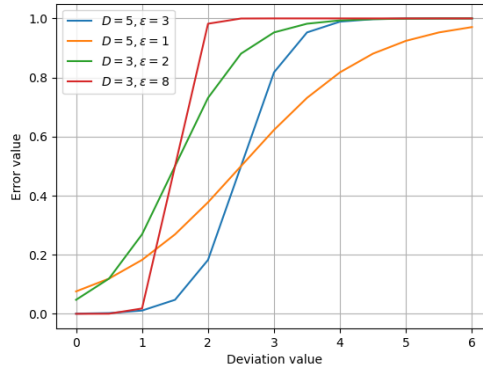
2. Evaluation of conformance over the entire route

The second category of conformance evaluation expands on the previous method by examining the simulation recorded points over the entire simulation and returning a single value. The first assigns a scaled value between 0 and 1 for each recorded point and returns the average over these points. This method is illustrated in Equations 3 and 4 where, D is the threshold distance, d is the distance from a given point to the flight plan trajectory segment, N is the total number of recorded points and ε is a growth variable where $\varepsilon >= 1$.

$$E = \frac{1}{1 + e^{\varepsilon\left(d - \frac{D}{2}\right)}} \tag{3}$$

$$E^{Route} = \frac{1}{N} \sum_{i=1}^{N} E_i \tag{4}$$

This approach gives the user control over how conservatively to consider deviation values while accounting loosely for uncertainties in position from the simulation. Illustrated in Figure 3 are varying values of the threshold distance D and scaling variable ε for values of d between 0 and 6. It should also be emphasized that E is always positive and $E \geq 0$.

Fig. 3 **The s-curves demonstrate the relative returned values for varying threshold values D and scaling variable ε, which affect how aggressively the curve is applied.**

3. Statistical evaluation of conformance over finite time intervals

The final method examines, for a given finite time interval, what is the probability of observing a deviation greater than the given threshold D. The mean (μ) and standard deviation (σ) is calculated over the time interval window and are used in the generation of the z-score in Equation 5. This is then used in Equation 6, to obtain the probability of observing a deviation greater or equal to the threshold D, where Φ is the cumulative distribution function of the standard normal distribution.

$$z = \frac{D - \mu}{\sigma} \tag{5}$$

$$P(d \geq D) = 1 - \Phi(z) \tag{6}$$

This approach, like (1) can be evaluated in tandem with the simulation improving efficiency. This does mean that, in conjunction with the deviation threshold D a secondary threshold needs to be introduced relating to the probability of observing a deviation greater than the threshold. Additionally, the time interval to perform this evaluation over is introduced as a further variable for this approach.

V. Predicting the Impact of Wind on Battery Energy

Our aim in the battery energy-related mission success/failure prediction process is to predict the occurrence of the battery's EoD, which is defined as the time at which the SoC of the battery falls below a pre-defined threshold value.

SoC of a battery is typically defined as 1 when the battery is fully charged and 0 when the battery is discharged to a predetermined voltage threshold. Such a task is known as prognostics, and we adopted model-based prognostics architecture from [33]. The architecture is summarized as follows:

Given a system model defined as:

$$x(k+1) = f(k, x(k), \theta(k), u(k), v(k)), \tag{7}$$

$$y(k) = h(k, x(k), \theta, u(k), n(k)), \tag{8}$$

where k is the discrete time variable, $x(k) \in R^{n_x}$ is the sate vector, $\theta(k) \in R^{n_\theta}$ is unknown parameter vector, $u(k) \in R^{n_u}$ is the input vector, $v(k) \in R^{n_v}$ is the process noise vector, f is the state equation, $y(k) \in R^{n_y}$ is the output vector, $n(k) \in R^{n_n}$ is the measurement noise vector, and h is the output equation.

The battery model utilized in this study is an electro-chemical-based model of Lithium-ion batteries, as described in [33], which are a popular choice for powering unmanned aerial vehicles. In this model, the battery's current draw (I) serves as the input, while the battery temperature (tb) and the voltage drop caused by solid-phase ohmic resistance (V_o) represent its outputs ($y(k)$).

The prognostics architecture comprises two major steps: estimation and prediction. the joint state-parameter estimate $p(x(k), \theta(k)|y(k_0 : k))$ is computed using the system dynamics and observation history up to time k represented as $y(k_0 : k)$. On the other hand, in the prediction step, the probability distribution $p(k_E(k_P)|y(k_0 : k_P))$ at prediction time k_p is computed using the joint state-parameter estimate and hypothesized future inputs of the system. The estimation algorithm used in this paper is the Unscented Kalman Filter (UKF) [34], along with the battery model. The UKF uses sigma points which are deterministic points that are used to represent the joint state-parameter distribution $p(x(k), \theta(k), |y(k_0 : k))$. The predictor algorithm used in this paper is the Monte Carlo predictor [35], which randomly samples from the battery's current state distribution, and each sample is simulated to the EoD. By collecting a set of EoD points from several Monte Carlo simulations, the probability distribution can be built, and the probability of mission success at a given time can be computed using the following equation:

$$P_{success}(time) = \frac{\sum_{i=1}^{n}(EOD(i) > time)}{n} \tag{9}$$

n represents the number of Monte Carlo simulations in the prediction step.
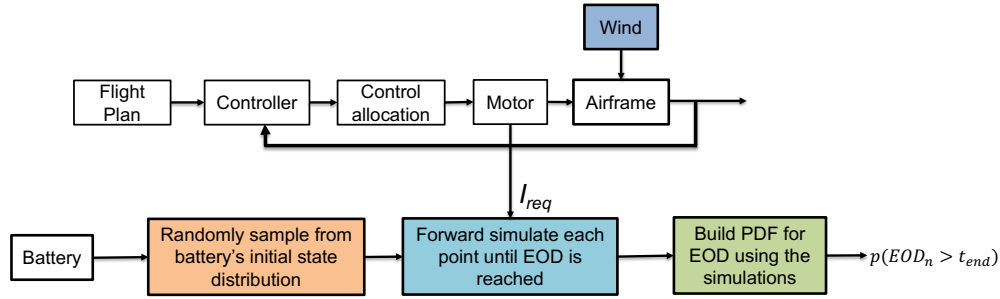
Fig. 4   Schematic diagram representation of the battery EoD prediction procedure

The battery EoD prediction process is illustrated in Figure 4. According to the procedure, given a flight plan and information about the available battery energy, the first step is to obtain the wind forecast along the 4-D trajectory of the flight plan using the techniques discussed in section IV. After collecting the wind data, the aircraft is simulated along the flight plan to obtain the mission's current requirement (I_{req}), which is used as a future load for battery EoD prediction. Next, the UKF-based estimator is employed to obtain the initial state distribution of the battery. Once the initial state distribution of the battery is obtained, samples are randomly drawn from the distribution, and the EoD is predicted for each sample using the Monte Carlo predictor. Finally, the predicted EoD points are collected, and the probability density function for battery EoD at the flight end time is constructed.

VI. Experiments

Experiments were run using the simulation environment presented in [28] with the parameters from Table 1 for the Tarot T18 octocopter. The experiment was run on a predefined route (seen in Figure 5a), with varying wind speeds and directions, defined in each experiment section.

A. Conformance Metric

As mentioned in Section IV, three approaches were identified as possible methods to evaluate deviation. To perform this evaluation a deviation threshold was set $D = 5$. For repeatability and to ensure a range of wind values were tested four scenarios, including the baseline *No Wind* scenario were generated, based on real wind data collected from an on-site testing location, in Centreville Virginia. The wind data was collected over two days: 10th April 2023 and 17th April 2023 with lower winds being observed on the 10th April and used for the *Low Winds* scenario. These winds represent low altitude operations under a 15-meter ceiling, the mean speeds and wind directions are found in Table 3. Additionally, forecast wind data was used in a second set of simulations. This data contains more consistent wind speeds but gusts are not naturally included. The forecast data, generated for 20th April 2021 was sampled over the Dallas Fort-Worth area.

1. Experimental results for a strict conformance boundary

The first approach described a hard, or *strict*, boundary where, if the aircraft deviated beyond the threshold value D, the simulation would terminate with a "non-conforming" result. In this scenario the simulation exited early, after the first waypoint because of a deviation after the first turn. In actuality the simulation exited all simulations close to this point.

Illustrated in Figure 5b is the entire *No Wind* simulation with points $d >= D$ outlined in red. Though normally the simulation would exit after the first deviation in this scenario it was run to completion as to provide an informative baseline over the entire route.

(a)   **(b)**
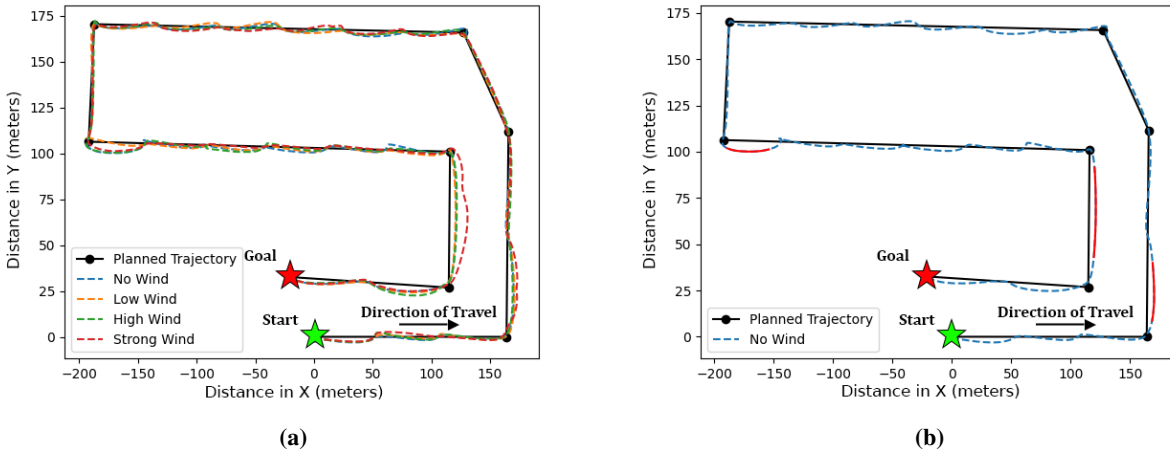
Fig. 5   (a) Shows all the wind scenarios tested over the prescribed trajectory. (b) Highlights the deviations, when $D = 5$ (red) for the no wind trajectory.

2. Experimental results for the evaluation of conformance over the entire route

The second approach attempts to quantify the probability of deviation over the entire simulation. That is, given a series of recorded points and the predefined set of waypoints, how many of those points exceed the deviation threshold for the flight. For this experiment the value of ε was set to 3 and D remained at 5. The results for the deviation values are presented in Table 3.

It was found that in scenarios with some wind the vehicle appears more stable in flight than in the complete absence of wind, this is illustrated by the probability of deviation dropping in the scenarios where any amount wind is being applied. We believe that this is due to the aircraft model's approach to control, hypothesizing that, in the absence of

wind, the aircraft's controller is only correcting for navigational errors. In cases of over correction, or frequent smaller corrections, as the aircraft attempts to maintain a perfect course, the aircraft appears to become unstable resulting in deviation. However, in cases with wind, the controller is primarily correcting based on the resultant forces from the observed winds rather than minor errors along the trajectory. Furthermore, as depicted in Figure 5a, even in the presence of winds there is very little effect on the overall trajectory of the aircraft. It can be noted that in the *Strong Winds* scenario the aircraft deviates more towards the end of the route which could be explained by observing more gusts near or above the safe upper wind speed limit, which, for the T18, is around $15 m/s$.

Additionally, this experiment, while it identified little change in the deviation of the aircraft, showed that overall flight time can be affected by wind speed significantly. Highlighted more by the *High Winds* and *Strong Winds* scenarios in Table 3, with a south-westerly wind the aircraft reduces the flight time significantly from a south-easterly wind. While the aircraft never experiences a direct head or tail wind for prolonged portions of flight this 10° variance in wind direction is enough to reduce flight time by ≈ 36 seconds.

Table 3   The flight times, in seconds, and mean probability of deviation (Equation 4) for each wind scenario

Scenario	Mean Wind Speed (m/s)	Mean Direction (deg)	Probability of Deviation	Flight Time (Seconds)
No Wind	0	0	0.235	504
Low Winds	2	210	0.197	488
High Winds	10	170	0.232	494
Strong Winds	15	230	0.227	458

In Table 4 the results from the forecast winds are demonstrated. Notably, when compared to the low altitude real scenarios mentioned previously, the probability of deviation increases significantly even at lower wind speeds. This is likely due to two factors. The first could be due to the direction of the wind, as seen in Table 3, with the mean direction below 200°, an increase in deviation probability was observed. This however is unlikely to be the sole isolating factor. The wind speeds observed in the forecast data were more consistent, that is, where in the real-world data both wind speed and direction fluctuated over short periods of time and was sampled at 10 second intervals, the forecast data was sampled at 15-minute intervals. Longer intervals between samples, in conjunction with interpolation to transition between values, results in less fluctuations in both wind speed and direction. During the times forecast for the flights, the wind speeds and directions varied only marginally, this likely resulted in the aircraft struggling to contend with the resultant sustained speeds and directions. We would also expect to see higher power consumption as a result of this.

Table 4   The flight times, in seconds, and mean probability of deviation (Equation 4) for each forecast wind scenario

| Scenario	Mean Wind Speed (m/s)	Mean Direction (deg)	Probability of Deviation	Flight Time (Seconds)
No Wind	0	0	0.235	504
Forecast 1	7.2	185	0.542	472
Forecast 2	10.43	192	0.520	477
Forecast 3	13.71	190	0.508	471

3. Experimental results for statistical evaluation of conformance over finite time intervals

In this approach a statistical evaluation was performed using the z-score for a discrete time interval during the simulation execution. The value returned is the probability of observing a deviation $d >= D$ at that interval. The graph in Figure 6a, shows the probabilities obtained when applied to the various wind scenarios mentioned above. As mentioned in Section IV, two new variables are introduced: the probability threshold, set to 0.9 here; and the interval used to predict deviations, in which we used 15 seconds. With these variables, this approach would consider all

scenarios to be valid except the latter *High Winds* and *Strong Winds* due to both breaking the threshold value.

This approach better quantifies the deviation probability at specific points of time. However, sudden spikes in deviation, such as those induced during wind gusts, poses a difficult case for this method if these spikes are short, i.e., not normally distributed. This induces some uncertainty in the results yielded through this approach as gust-induced deviation is obfuscated by the algorithm. Varying the probability threshold or time interval can accommodate to some lengths this issue but does not mitigate it in its entirety.

As seen in Section VI.A.2, the use of the forecast winds significantly affected the calculated probabilities, which is again observed here. In Figure 6b, it was observed that, in all experiments, using the forecast winds the aircraft regularly passed the deviation threshold of $D = 5$. When that threshold is increased by 2 meters (Figure 6c) it is revealed that the lower forecast speed scenarios perform worse than the higher speed scenario. It is not known what the cause of this discrepancy is although, it is possible that the "over correction error", discussed in Section VI.A.2, could be partially responsible for the excessive deviations in lower wind speeds.

(a)

(b)

(c)
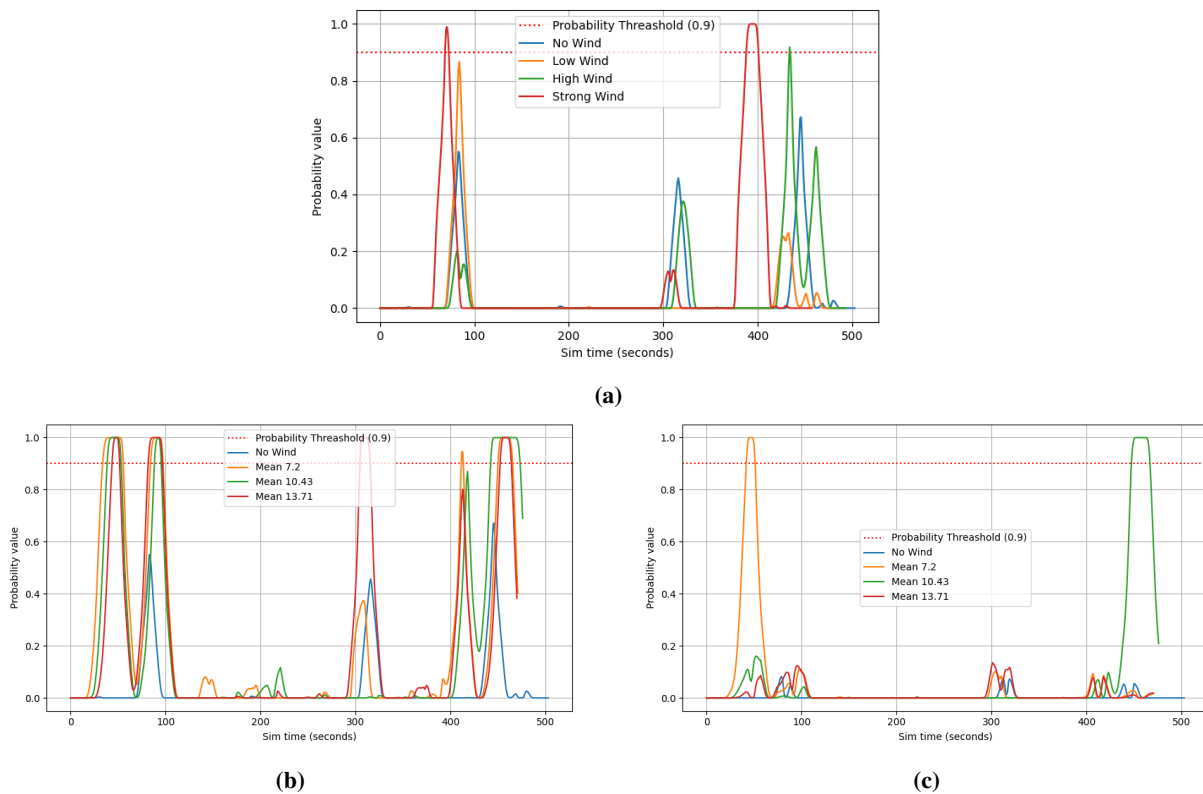
Fig. 6 **The probability of observing a deviation $d >= D$ for the different wind scenarios over a time interval of 15 seconds and $D = 5$. (a) Shows the probabilities for wind data collected on site; (b) shows the probabilities for the forecast winds and (c) shows the probabilities for forecast winds when $D = 7$.**

B. Battery Experiments

In this sub-section, we present the experimental setup we adopt to investigate the impact of wind on battery energy consumption and the success of flight missions. We utilized the same flight plan and wind data as the conformance-related experiments in Section VI.A. We conducted four sets of experiments, each with varying wind forecasts, to observe differences in the effect of wind on battery energy consumption. The results of these experiments, including the specific wind conditions and their corresponding impact on mission success, are presented in Table 5. To determine the probability of mission success or failure, we established a threshold SoC value of 25% at the end of the flight. If the SoC value for a given flight plan falls below 25%, we consider the mission a failure, while if it is above this value, we consider it safe.

10

Table 5 Wind Conditions and Their Impact on Probability of Mission Success in Battery-Related Experiments

Scenario	Mean Wind Speed (m/s)	Mean Direction (deg)	Probability of Mission Success	Flight Time (Seconds)
No Wind	0	0	1	311
Forecast 1	7.2	185	1	311
Forecast 2	10.43	192	0.57	514
Forecast 3	13.71	190	0	582

Figure 7 presents the output voltage and SoC predictions, resulting from 500 Monte Carlo simulations, as recommended in [24]. The first experiment is represented in Figures 7a and 7d, where the aircraft operates in the presence of low wind speeds. All the SoC predictions of the battery in Figure 7d exceed the threshold value of 25%, indicating a probability of mission success of 1. For the second case study, we simulated the aircraft operating at high wind speeds and present the voltage and SoC predictions in Figures 7b and 7e, respectively. In this case, a portion of the Monte Carlo simulations resulted in an SoC value below the threshold, while others were above it. Therefore, we can compute the probability of mission success using Equation 9, resulting in a probability of 0.57. Finally, we conducted the experiment in the presence of strong wind, and the outcomes are shown in Figures 7c and 7f. From Figure 7f, it is apparent that all SoC predictions are below the threshold value. Thus, the probability of mission success in this scenario is 0. Based on the results, it can be inferred that an increase in wind speed leads to a rise in aircraft battery energy consumption, consequently resulting in a decrease in mission success probability.

(a)   **(b)**   **(c)**

(d)   **(e)**   **(f)**
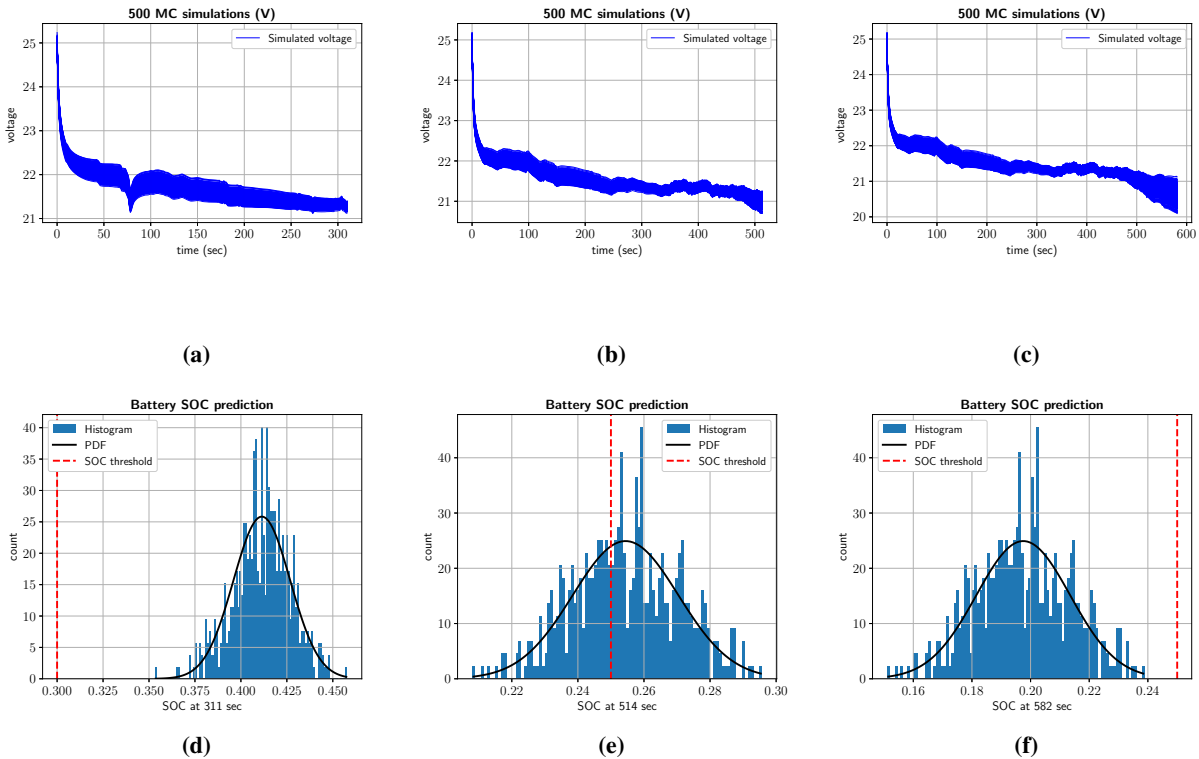
Fig. 7 (a), (b) and (c) show the output voltage profiles in the presence of low, high, and strong winds, respectively. (d), (e) and (f) show the SoC predictions in the presence of low, high, and strong winds.

VII. Conclusion

In this paper we presented work on evaluating conformance for flight plan feasibility in the presence of wind considering both: deviation due to wind and battery SoC. For evaluating conformance with wind-induced deviations, three approaches were presented examining strict-bound conformance, conformance evaluation over the entire route and a statistical approach using discrete finite time intervals. To evaluate battery energy-related mission success probability, a model-based prognostics architecture is utilized.

Results from the deviation evaluation found that, in the 4 given scenarios, there is little variation overall in the trajectories derived from the simulation in the presence of wind. It was found however that, with wind, the simulated aircraft is both more stable and, for the given scenarios, can complete the route in less time. The latter of the three proposed approaches is favored in its approach due to the ability to capture the probability of deviation at discrete time intervals. Even with the diminished performance in scenarios with high gust-induced deviation, this approach has better perceived scalability. We proposed that by modifying the threshold variables and interval variable gusts could be better represented or the approach can be better adapted for different stages of flight. Furthermore, we can hypothesize that learning based methods, such as regression-based techniques, or optimization techniques, could be adapted to either improve the threshold and interval variables or probabilistically predict deviations out right.

The experiments related to battery energy consumption reveal that flying the aircraft in windy conditions leads to an increase in battery energy consumption due to the vehicle's compensation for the wind's impact. Consequently, the probability of mission success decreases as the wind speed increases. Therefore, the presented framework can be utilized to facilitate the pre-departure decision-making process by estimating the probability of mission success under specific flight conditions and battery states of charge.

Future work will look at the inclusion of ensemble forecasts to aid in the feasibility evaluation. These ensemble forecasts will consist of multiple, potential observations with even probability distributions, e.g., ten forecasts each with a probability value of 0.1. With the ensemble forecasts a broader range of possible wind profiles can be evaluated for a single flight plan reducing the uncertainty that is present with just a single wind profile, we anticipate a more robust analysis by extension.

VIII. Acknowledgments

References

[1] Thompson, E. L., Taye, A. G., Guo, W., Wei, P., Quinones, M., Ahmed, I., Biswas, G., Quattrociocchi, J., Carr, S., Topcu, U., Jones, J. C., and Brittain, M. W., "A Survey of eVTOL Aircraft and AAM Operation Hazards," *AIAA AVIATION 2022 Forum*, 2022. https://doi.org/10.2514/6.2022-3539.

[2] Quinones-Grueiro, M., Biswas, G., Ahmed, I., Darrah, T., and Kulkarni, C., "Online decision making and path planning framework for safe operation of unmanned aerial vehicles in urban scenarios," *International Journal of Prognostics and Health Management*, Vol. 12, No. 3, 2021.

[3] Pradeep, P., Lauderdale, T. A., Chatterji, G. B., Sheth, K., Lai, C. F., Sridhar, B., Edholm, K.-M., and Erzberger, H., "Wind-Optimal Trajectories for Multirotor eVTOL Aircraft on UAM Missions," *AIAA AVIATION 2020 FORUM*, 2020. https://doi.org/10.2514/6.2020-3271.

[4] Bahr, M., Hebbar, U., Ferede, E., and Farhan, G., "Multi-rotor eVTOL Flight Simulation and Assessment under Atmospheric Turbulence," *Vertical Flight Society's 77th Annual Forum & Technology Display*, 2021.

[5] D'Souza, S. N., *Developing a Generalized Trajectory Modeling Framework for Small UAS Performance in the Presence of Wind*, 2017. https://doi.org/10.2514/6.2017-0447, URL https://arc.aiaa.org/doi/abs/10.2514/6.2017-0447.

[6] Choi, H. S., Lee, S., Ryu, H., Shim, H., and Ha, C., "Dynamics and Simulation of the Effects of Wind on UAVs and Airborne Wind Measurement," *Transactions of the Japan Society for Aeronautical and Space Sciences*, Vol. 58, No. 4, 2015, pp. 187–192. https://doi.org/10.2322/tjsass.58.187.

[7] Chalk, C. R., Neal, T. P., Harris, T. M., Pritchard, F. E., and Woodcock, R. J., "Background Information and User Guide for Mil-F-8785B (ASG), 'Military Specification-Flying Qualities of Piloted Airplanes'," 1969.

[8] Foster, J. V., and Hartman, D., "High-Fidelity Multi-Rotor Unmanned Aircraft System (UAS) Simulation Development for Trajectory Prediction Under Off-Nominal Flight Dynamics," *17th AIAA Aviation Technology, Integration, and Operations Conference*, 2017. https://doi.org/10.2514/6.2017-3271.

[9] Hartman, D., "Identification of Hazardous Flight Conditions to Establish a Safe Flight Envelope for Autonomous Multirotor Aircraft," *AIAA Scitech 2019 Forum*, 2019. https://doi.org/10.2514/6.2019-1292.

[10] Altamirano, G., and McCrink, M., "Investigation of Longitudinal Aero-Propulsive Interactions of a Small Quadrotor Unmanned Aircraft System," *AIAA Scitech 2021 Forum*, 2021. https://doi.org/10.2514/6.2021-1310.

[11] Mcnally, D., Sheth, K., Gong, C., Love, J. F., Lee, C. H., Sahlman, S., and Cheng, J.-H., "ynamic weather routes: a weather avoidance system for near-term trajectory-based operations," *28th International Congress of the Aeronautical Sciences*, 2012, pp. 23–28.

[12] Erzberger, H., Nikoleris, T., Paielli, R. A., and Chu, Y.-C., "Algorithms for control of arrival and departure traffic in terminal airspace," *Proceedings of the Institution of Mechanical Engineers, Part G: Journal of Aerospace Engineering*, Vol. 230, No. 9, 2016, pp. 1762–1779. https://doi.org/10.1177/0954410016629499.

[13] Erzberger, H., Lauderdale, T. A., and Chu, Y.-C., "Automated conflict resolution, arrival management, and weather avoidance for air traffic management," *Proceedings of the Institution of Mechanical Engineers, Part G: Journal of Aerospace Engineering*, Vol. 226, No. 8, 2012, pp. 930–949. https://doi.org/10.1177/0954410011417347.

[14] Pang, Y., Yao, H., Hu, J., and Liu, Y., *A Recurrent Neural Network Approach for Aircraft Trajectory Prediction with Weather Features From Sherlock*, 2019. https://doi.org/10.2514/6.2019-3413.

[15] Sherali, H. D., Staats, R. W., and Trani, A. A., "An Airspace Planning and Collaborative Decision-Making Model: Part I—Probabilistic Conflicts, Workload, and Equity Considerations," *Transportation Science*, Vol. 37, No. 4, 2003, pp. 434–456.

[16] Zoutendijk, M., and Mitici, M., "Probabilistic Flight Delay Predictions Using Machine Learning and Applications to the Flight-to-Gate Assignment Problem," *Aerospace*, Vol. 8, No. 6, 2021. https://doi.org/10.3390/aerospace8060152.

[17] Bongiorno, C., Gurtner, G., Lillo, F., Mantegna, R., and Miccichè, S., "Statistical characterization of deviations from planned flight trajectories in air traffic management," *Journal of Air Transport Management*, Vol. 58, 2017, pp. 152–163. https://doi.org/https://doi.org/10.1016/j.jairtraman.2016.10.009.

[18] Swenson, H. N., Hoang, T., Engelland, S., Vincent, D., Sanders, T., Sanford, B., and Heere, K., "Design and Operational Evaluation of the Traffic Management Advisor at the Fort Worth Air Route Traffic Control Center," , 1997.

[19] Davis, T. J., Isaacson, D. R., Robinson III, J. E., denBraven, W., Lee, K. K., and Sanford, B., "Operational test results of the passive final approach spacing tool," , 1997.

[20] Ayhan, S., and Samet, H., "Aircraft Trajectory Prediction Made Easy with Predictive Analytics," *Proceedings of the 22nd ACM SIGKDD International Conference on Knowledge Discovery and Data Mining*, Association for Computing Machinery, New York, NY, USA, 2016, p. 21–30. https://doi.org/10.1145/2939672.2939694.

[21] de Leege, A., van Paassen, M., and Mulder, M., *A Machine Learning Approach to Trajectory Prediction*, 2013. https://doi.org/10.2514/6.2013-4782.

[22] Sweet, A., Gorospe, G., Daigle, M., Balaban, E., Roychoudhury, I., Narasimhan, S., et al., "Demonstration of prognostics-enabled decision making algorithms on a hardware mobile robot test platform," *Annual Conference of the PHM Society*, Vol. 6, 2014.

[23] Daigle, M., and Kulkarni, C. S., "End-of-discharge and end-of-life prediction in lithium-ion batteries with electrochemistry-based aging models," *AIAA Infotech@ aerospace*, 2016, p. 2132.

[24] Corbetta, M., and Kulkarni, C. S., "An approach for uncertainty quantification and management of unmanned aerial vehicle health," *Annual PHM Society Conference*, 2019.

[25] Pradeep, P., and Wei, P., "Energy-efficient arrival with rta constraint for multirotor evtol in urban air mobility," *Journal of Aerospace Information Systems*, Vol. 16, No. 7, 2019, pp. 263–277.

[26] Pradeep, P., Lauderdale, T. A., Chatterji, G. B., Sheth, K., Lai, C. F., Sridhar, B., Edholm, K.-M., and Erzberger, H., "Wind-optimal trajectories for multirotor eVTOL aircraft on UAM missions," *Aiaa Aviation 2020 Forum*, 2020, p. 3271.

[27] Schumann, J., Kulkarni, C., Lowry, M., Bajwa, A., Teubert, C., and Watkins, J., "Prognostics for Autonomous Electric-Propulsion Aircraft," *International Journal of Prognostics And Health Management*, Vol. 12, No. 3, 2021.

[28] Ahmed, I., Quinones-Grueiro, M., and Biswas, G., "A high-Fidelity Simulation test-Bed for fault-Tolerant octo-Rotor Control Using Reinforcement Learning," *2022 IEEE/AIAA 41st Digital Avionics Systems Conference (DASC)*, IEEE, 2022.

[29] Tarot-Rc, "Tarot T18 UAV Oct-copter Frame Set TL18T00," , 2022. URL https://www.tarot-rc.com/tarot-t18-uav-oct-copter-frame-set-tl18t00-p2562477.html, accessed 16 April 2023.

[30] Skamarock, W. C., Klemp, J. B., Dudhia, J., Gill, D. O., Liu, Z., Berner, J., Wang, W., Powers, J. G., Duda, M. G., Barker, D. M., and Huang, X. Y., "A description of the advanced research WRF model version 4," Tech. rep., 2019. National Center for Atmospheric Research: Boulder, CO, USA, NCAR/TN-556+STR.

[31] Tarot-Rc, "Tarot Multirotor UAV/8-Axis/Training Exercise frame X8-Lite," , 2022. URL https://www.tarot-rc.com/tarot-multirotor-uav8-axistraining-exercise-frame-x8-lite-p4196269.html, accessed 16 April 2023.

[32] FAA, "90-105A Approval Guidance for RNP Operations and Barometric Vertical Navigation in the U.S. National Airspace System and in Oceanic and Remote Continental Airspace," , 2016. URL https://www.faa.gov/regulations_policies/advisory_circulars/index.cfm/go/document.information/documentid/1029146.

[33] Daigle, M., and Kulkarni, C. S., "Electrochemistry-based battery modeling for prognostics," *Annual Conference of the PHM Society*, Vol. 5, 2013.

[34] Wan, E. A., and Van Der Merwe, R., "The unscented Kalman filter," *Kalman filtering and neural networks*, 2001, pp. 221–280.

[35] Ekwaro-Osire, S., Gonçalves, A. C., Alemayehu, F. M., et al., *Probabilistic prognostics and health management of energy systems*, Springer, 2017.